

AI-Powered Intracranial Hemorrhage Detection: A Co-Scale Convolutional Attention Model with Uncertainty-Based Fuzzy Integral Operator and Feature Screening

Mehdi Hosseini Chagahi, Niloufar Delfan, Behzad Moshiri, Md. Jalil Piran, Jaber Hatam Parikhan

Abstract—Intracranial hemorrhage (ICH) refers to the leakage or accumulation of blood within the skull, which occurs due to the rupture of blood vessels in or around the brain. If this condition is not diagnosed in a timely manner and appropriately treated, it can lead to serious complications such as decreased consciousness, permanent neurological disabilities, or even death. The primary aim of this study is to detect the occurrence or non-occurrence of ICH, followed by determining the type of subdural hemorrhage (SDH). These tasks are framed as two separate binary classification problems. By adding two layers to the co-scale convolutional attention (CCA) classifier architecture, we introduce a novel approach for ICH detection. In the first layer, after extracting features from different slices of computed tomography (CT) scan images, we combine these features and select the 50 components that capture the highest variance in the data, considering them as informative features. We then assess the discriminative power of these features using the bootstrap forest algorithm, discarding those that lack sufficient discriminative ability between different classes. This algorithm explicitly determines the contribution of each feature to the final prediction, assisting us in developing an explainable AI model. The features feed into a boosting neural network as a latent feature space. In the second layer, we introduce a novel uncertainty-based fuzzy integral operator to fuse information from different CT scan slices. This operator, by accounting for the dependencies between consecutive slices, significantly improves detection accuracy.

Index Terms—Vision transformer, Uncertainty-based fuzzy integral operator, Intracranial hemorrhage, Explainable AI, Boosting neural network.

I. INTRODUCTION

ICH, recognized as one of the most critical and life-threatening medical conditions, can severely impact patient health and require prompt and accurate diagnosis in order to ensure appropriate treatment [1], [2]. These types of hemorrhages are typically caused by traumatic injuries, such as head trauma, or specific medical conditions like aneurysm rupture, high blood pressure, or blood disorders [3], [4]. This

M. H. Chagahi and N. Delfan are with the School of Electrical and Computer Engineering, College of Engineering, University of Tehran, Tehran, Iran, (e-mail: mehdichagahi@gmail.com; niloufardelfan@gmail.com)

B. Moshiri is with the School of Electrical and Computer Engineering, College of Engineering, University of Tehran, Tehran, Iran and the Department of Electrical and Computer Engineering University of Waterloo, Waterloo, Canada, (e-mail: moshiri@ut.ac.ir)

M. J. Piran is with the Department of Computer Science and Engineering, Sejong University, Seoul 05006, South Korea, (e-mail: piran@sejong.ac.kr)

J. H. Parikhan is with the Department of Neurosurgery, Iran University of Medical Sciences

emergency situation can rapidly increase intracranial pressure and cause damage to brain tissues [5], [6].

In the past, diagnosing such hemorrhages primarily relied on conventional imaging techniques, such as CT scans and magnetic resonance imaging (MRI). These images were reviewed by radiologists and neurologists to determine the type and severity of the hemorrhage [7], [8]. However, due to the reliance on the expertise and experience of physicians, these methods have always faced challenges related to accuracy and speed [9], [10].

In the past decade, with significant advancements in artificial intelligence and machine learning (ML), research has shifted towards the development of automated models for the detection and classification of intracranial hemorrhages [11]–[14]. Deep learning (DL) models, such as convolutional neural networks (CNNs), pre-trained networks, and attention-based architectures, have garnered considerable attention from researchers due to their high capability in analyzing medical images [15]–[20]. These models can automatically analyze CT scan images and accurately detect ICH.

The study [21] presented a novel method for Multiple Instance Learning (MIL) for medical image analysis, particularly for detecting ICH in CT scans. The approach built on Gaussian Process-based MIL (VGPMIL) but introduced a new formulation using Pólya-Gamma random variables to handle the logistic function more efficiently. The reformulation, called PG-VGPMIL, was mathematically equivalent to the original VGPMIL model but provided better computational tractability.

Perez et al. [22], presented a novel end-to-end model combining CNN, attention mechanisms, and gaussian processes for MIL to detect ICH from CT scans. The method overcame challenges in the manual annotation of large datasets by using scan-level labels instead of slice-level labels. The CNN was employed to extract features from each CT slice, which were then processed by an attention mechanism that assigned weights to highlight important slices. These weighted feature vectors were passed into a sparse gaussian process for probabilistic classification.

The work [23] evaluated a novel DL algorithm based on the Dense-UNet architecture for detecting ICH in non-contrast CT (NCCT) head scans after traumatic brain injury. The algorithm processed CT scans by segmenting the brain using anatomical landmarks and performed volumetric segmentation to detect hemorrhage. The algorithm used a 3D Dense-UNet

architecture, which introduced densely connected layers to enhance segmentation quality by allowing each layer to receive inputs from all previous layers and pass outputs to subsequent layers.

Sindhura et al. [24] proposed a fully automated sinogram-based DL model for the classification of ICH directly from sinogram data, eliminating the need for the time-consuming reconstruction phase of CT scans. The method involved a two-stage approach: the first stage used a U-Net-based model to synthesize sinograms equivalent to intensity-windowed CT scans that are commonly used in brain imaging. The second stage was a detection module composed of a CNN and a recurrent neural network (RNN), where the CNN extracted features from the sinograms, and the RNN (Bi-GRU) captured spatial information across neighboring slices to improve accuracy in detecting hemorrhages.

Shah and Jaimin [25] evaluated the usability and human factor engineering of a ML-powered Near-Infrared Spectroscopy (mNIRS) device, designed for point-of-care detection of ICH in patients with traumatic brain injury. The mNIRS device leveraged near-infrared light to non-invasively assess brain tissues, detecting extravascular bleeds by measuring light absorption and scattering through the scalp and skull.

The study [26] introduced a semi-supervised learning model for the detection and segmentation of ICH from head CT scans. The proposed method combined labeled and unlabeled data to improve model generalizability, particularly on out-of-distribution datasets. The semi-supervised model showed significant improvements in generalizability compared to a fully supervised baseline model, achieving higher accuracy in both classification (AUC 0.939 vs. 0.907) and segmentation (Dice similarity coefficient of 0.829 vs. 0.809).

Ragab and Mahmoud [27] introduced the political optimizer (PO) with deep learning for ICH Diagnosis. The method began with bilateral filtering for preprocessing CT images, which helped in removing noise while preserving the edges. For feature extraction, the Faster SqueezeNet model was used to capture relevant features from the images. Finally, a denoising autoencoder model was employed for classification, with hyperparameter optimization performed by the PO algorithm.

The work [28] proposed a DL model for ICH detection using CT scans. The model was based on a combination of two neural network architectures: ResNet and EfficientDet. ResNet addressed challenges such as vanishing or exploding gradients, while EfficientDet focused on computational efficiency through its novel Bi-directional feature pyramid network and compound scaling method. Together, these architectures formed the backbone of the model, which optimized detection accuracy while minimizing computational resources. Li et al. [29] introduced a novel DL-enabled microwave-induced thermoacoustic tomography (MITAT) technique, leveraging a residual attention U-Net architecture for transcranial brain hemorrhage detection. The method addressed challenges related to acoustic inhomogeneity caused by the skull during transcranial imaging. MITAT combined microwave irradiation with thermoacoustic effects to capture tissue contrast and generate high-resolution brain images. Unlike previous studies that selectively utilized only a few slices from CT

scan images to detect ICH, this study, inspired by real-world practices, integrates all informative slices from a CT scan using a uncertainty-based fuzzy integral operator. This approach enables the development of a more robust and reliable detection model. By employing feature selection and combination techniques to create a latent feature space, the proposed model focuses solely on the features with the highest contribution to the final prediction. This approach significantly reduces computational costs and facilitates the development of an interpretable model.

- A large dataset comprising head CT scan images from two medical centers is collected and meticulously labeled.
- Data preprocessing involves the removal of heterogeneous color regions and the reduction of image dimensions to focus on the primary brain tissue using background subtraction and binary masking techniques.
- Permutation technique is employed to assess the importance of each feature, allowing for the identification and removal of features that lack sufficient discriminative power.
- An uncertainty-based fuzzy integral operator is introduced, capable of combining multiple CT scan slices for enhanced diagnostic accuracy.

The structure of this study is: Section II summarizes the dataset, highlighting image preprocessing. It then discusses the processes of feature fusion and feature importance, concluding with an in-depth analysis of the proposed system's architecture. Section III presents the findings and their analysis. Section IV explores potential avenues for future research. Finally, Section V offers concluding remarks.

II. FUZZY-BASED ICH DETECTION FRAMEWORK

Fig. 1 illustrates the overall architecture of the proposed system for detecting ICH and SDH. Initially, the raw images undergo essential preprocessing. Following this, feature extraction is performed, and subsequently, feature fusion and selection techniques apply to ensure that only the most discriminative features are kept for input to the boosting neural network. The architecture estimates the probability of each slice belonging to specific classes. Finally, slices from the same CT scan are aggregated using a fuzzy integral operator based on uncertainty, resulting in the determination of the final label for the CT scan. In the following, we delve into the details of each component of the proposed system.

A. Data acquisition and labeling

In this study, we utilize two datasets: NICH137 and SDH45. The NICH137 dataset focuses on assessing the presence or absence of ICH, while the SDH45 dataset is dedicated to identifying the type of Subdural Hemorrhage. Please see Table I for a comprehensive overview of the two datasets. Both datasets were collected between 2018 and 2024 from two medical centers in Tehran: Rasul Akram Hospital and Firouzabadi Hospital. They were meticulously labeled by two board-certified neurosurgeons. Labeling was initially performed by a board-certified neurosurgeon and subsequently validated by another board-certified neurosurgeon who is also a university

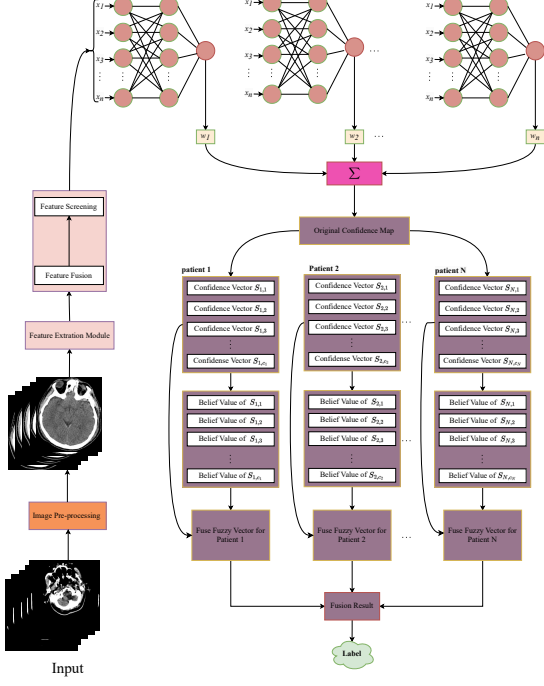


Fig. 1. The proposed architecture for detecting ICH.

faculty member. Fig. 2 shows two slices from two classes: normal (no hemorrhage) and ICH (presence of at least one type of hemorrhage). Additionally, Fig. 3 presents two slices from two classes: Acute Subdural Hemorrhage (ASDH) and Chronic Subdural Hemorrhage (CSDH). Differentiating these two types of hemorrhage is crucial, as they require distinct management and treatment approaches.

The dataset includes brain CT scans acquired using two protocols: parenchymal view and bone view. For the purpose of ICH classification, we specifically employ the parenchymal view protocol. The CT scans are got using a Siemens scanner, with each scan comprising 25 to 40 slices at a thickness of 5 millimeters.

Only the axial view for ICH classification is used due to its accessibility, as axial views are the most readily available brain CT view, whereas coronal and sagittal reconstructions are time intensive.

This research project is registered as a proposal at the Iran University of Medical Sciences and received ethical approval under code number —. The researchers are committed to adhering to ethical principles in research and to following the Declaration of Helsinki.

B. Image preprocessing

The data preprocessing for preparing brain CT scan images for use in DL models is conducted in several stages. First, the head CT scan images are separated from all available images, which include various sections such as body, lungs, bones. Subsequently, these images are converted from DICOM format to the more commonly used JPEG format. At this stage, noisy slices or those lacking brain tissue are removed from the dataset to improve the quality of the input data for the models.

TABLE I
SUMMARY OF SAMPLE DISTRIBUTION ACROSS PATIENT GROUPS

Sample	Binary		Binary	
	Normal	ICH	ASDH	CSDH
Patient	63	74	24	21
CT scan	200	200	55	48
Slice	15796	15800	1550	1235

To enhance the focus of DL models on the primary brain tissue and information-rich areas, background removal techniques are initially applied to identify and eliminate non-homogeneous color regions in the images. Afterward, a binary mask is employed to dynamically crop the images. The resulting cropped images contain only the main brain tissue.

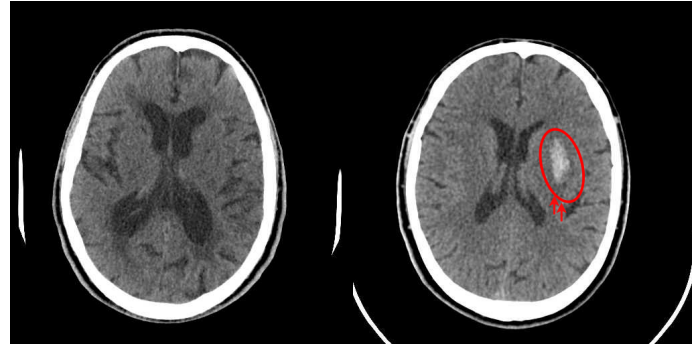
C. Feature Fusion and Feature Importance

Based on a comprehensive review of prior studies, DL models with the highest frequency and best performance in Q1-ranked publications are selected as the most suitable candidates for feature extraction from CT scan images. In our study dataset, the CCA and VGG19 models demonstrate the best performance in feature extraction, while the cross-attention and EfficientNetB6 models show the worst performance in this regard. To refine the extracted features, we apply principal component analysis (PCA) and select the top 50 components from each model that account for the greatest data variance, considering these as informative features. This transformation enables a shift from basic features to more sophisticated ones, effectively reducing feature dimensionality and substantially lowering computational costs. To evaluate the discriminative power of these components, the Bootstrap Forest algorithm is employed. This algorithm leverages permutation techniques to determine the importance of each component in the final prediction by iteratively permuting the values of each component while keeping others constant. The greater the effect of a component's permutation on model accuracy, the more critical that component is deemed to be. In fact, we define the Separation Index—often define as the ratio of intra-class to inter-class variance—as the component's impact on model accuracy.

Fig. 4 and Fig. 5 illustrate the importance of each component of the CCA model, identified as the best-performing model, in detecting ICH and SDH, respectively. Components contributing less than 1% to the overall performance were identified and excluded as non-discriminative. Consequently, 22 components were selected for ICH detection and 32 components for SDH detection, serving as the latent feature space to feed the boosting neural network.

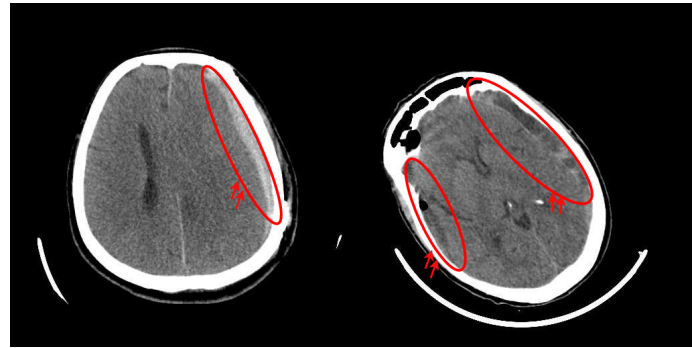
D. Boosting Neural Networks

After identifying the informative and discriminative features through PCA and permutation techniques, these features are



(a) CT scan of a normal brain
(b) CT scan of a brain with hemorrhage.

Fig. 2. (a) CT scan of a normal brain without any signs of hemorrhage, (b) CT scan of a brain with ICH, illustrating visible regions of bleeding.



(a) Brain CT scan showing ASDH
(b) Brain CT scan showing CSDH

Fig. 3. (a) Brain CT scan showing ASDH, characterized by recent bleeding with high-density regions, (b) Brain CT scan showing CSDH, indicating older, low-density blood accumulation.

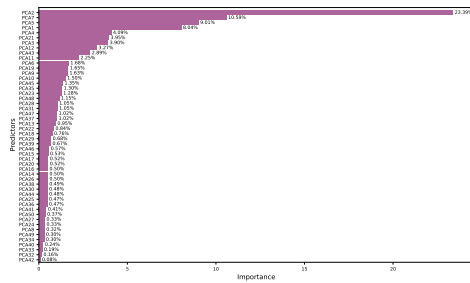


Fig. 4. Importance ranking of predictors based on their contribution to the ICH classification model.

fed into a boosting neural network. This architecture comprises 10 component models, each focusing on correcting the errors of its predecessor. The final outputs of the component models are combined in a weighted manner based on accuracy, generating a probability for each slice belonging to each class, referred to as the original confidence map. Table II details the hyperparameters of each component model. Our criterion for selecting 10 component models are based on starting with the minimum number of models and stopping when adding a new model component has a negligible effect on accuracy.

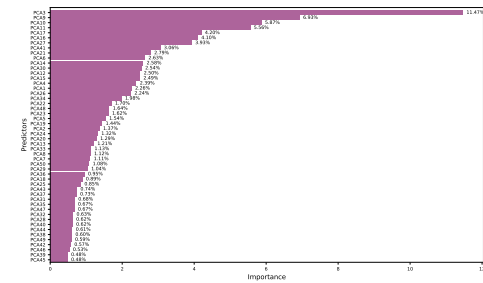


Fig. 5. Importance ranking of predictors based on their contribution to the SDH classification model.

Essentially, the number of component models represents a trade-off between complexity and performance.

E. uncertainty-based fuzzy integral operator

Since hemorrhage may not be visible in a single slice but could be apparent across consecutive slices, and single-slice diagnosis is highly susceptible to environmental variations such as changes in patient angle and position, analyzing multiple slices allows the AI system to examine a broader range of

TABLE II
HYPERPARAMETERS OF EACH COMPONENT MODEL IN THE BOOSTING
NEURAL NETWORK

Hidden Layers	Activation Function			Learning Rate	Epochs	Penalty Method
	Sigmoid	Identity	Radial			
L_1	25	10	15	0.1	100	Squared
L_2	10	5	10			

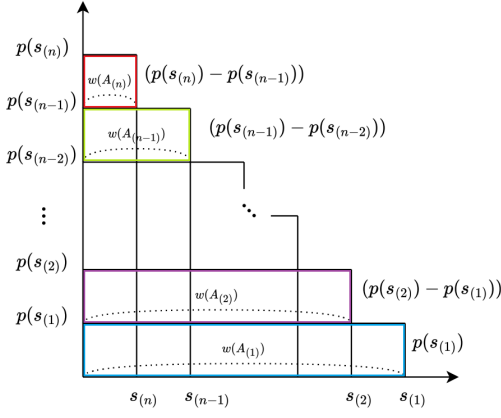


Fig. 6. Fuzzy integral operator framework for aggregation of diverse CT scan slices.

patterns, enhancing diagnostic accuracy. Therefore, to integrate multiple slices of a CT scan, we utilize an uncertainty-based fuzzy integral operator, which is capable of accounting for interactions among different slices and provides an adequate level of complexity [30], [31].

As illustrated in Fig. 6, consider a set

$S = \{s_1, s_2, s_3, \dots, s_n\}$ consisting of n slices with probabilities $p(s_1), p(s_2), p(s_3), \dots, p(s_n)$, ordered such that:

$$p(s_1) \leq p(s_2) \leq \dots \leq p(s_n), \quad p(s_0) = 0 \quad (1)$$

The fuzzy measures are denoted as

$w(A_1), w(A_2), \dots, w(A_n)$, and the parameter λ is computed according to (2).

$$\lambda + 1 = \prod_{i=1}^n (1 + \lambda \cdot w_\lambda(s_i)), \quad -1 < \lambda < +\infty \quad (2)$$

If $\sum_{i=1}^n w_\lambda(s_i) = 1$, $\lambda = 0$ is an acceptable value. When $\sum_{i=1}^n w_\lambda(s_i) < 1$, λ lies in the range $0 < \lambda < +\infty$. Conversely, if $\sum_{i=1}^n w_\lambda(s_i) > 1$, then λ is in the range $-1 < \lambda < 0$. The weight $w(s_i)$ represents the assigned weight for the i -th slice.

The area of the first rectangle is $p(s_1).w(A_1)$, where:

$$w(A_1) = w(\{s_1, s_2, s_3, \dots, s_n\}) = w(s_1) + w(s_2) + \dots + w(s_n) + \lambda \cdot w(s_1)w(s_2) \dots w(s_n) \quad (3)$$

The area of the second rectangle is $(p(s_2) - p(s_1)).w(A_2)$, where:

$$w(A_2) = w(s_2, s_3, \dots, s_n) = w(s_2) + w(s_3) + \dots + w(s_n) + \lambda \cdot w(s_2)w(s_3) \dots w(s_n) \quad (4)$$

Similarly, the area of the third rectangle is $(p(s_3) - p(s_2)).w(A_3)$, where:

$$w(A_3) = w(s_3, s_4, \dots, s_n) = w(s_3) + w(s_4) + \dots + w(s_n) + \lambda \cdot w(s_3)w(s_4) \dots w(s_n) \quad (5)$$

Finally, the area of the n -th rectangle is $(p(s_n) - p(s_{n-1})).w(A_n)$, where:

$$w(A_n) = w(s_n) \quad (6)$$

The total aggregated area can be expressed as:

$$\int p, dw = p(s_1) \cdot w(A_1) + (p(s_2) - p(s_1)) \cdot w(A_2) + \dots + (p(s_n) - p(s_{n-1})) \cdot w(A_n) \quad (7)$$

This is generalized for all slices using (8):

$$\int p, dw = \sum_{i=1}^n (p(s_i) - p(s_{i-1})) \cdot w(A_i) \quad (8)$$

The challenges associated with aggregating information from different CT slices using the standard fuzzy integral operator [32]–[34] are as follows:

Computing the Parameter λ : According to (2), if a CT scan consists of n slices, aggregating these slices using the fuzzy integral operator requires solving an n -degree equation. Since n may vary between different CT scans, $n \in \{c_1, c_2, \dots, c_N\}$ where c_k represents the number of slices in the k -th scan, each scan necessitates solving a unique equation of order n , leading to significant computational complexity.

Since $\sum_{i=1}^n w_\lambda(s_i) > 1$, to reduce the complexity, we treat λ as a hyperparameter within the range $-1 < \lambda < 0$ and optimize it using a grid search approach. This method eliminates the need for solving high-order equations while maintaining computational efficiency.

Assigning Weights to CT Scan Slices: In the standard version of the fuzzy integral operator, the weight assigned to each information source (different slices of a CT image) is determined by a domain expert. To determine the significance of each slice, we use uncertainty as the guiding principle. In classification models, high confidence in a class prediction (e.g., one probability close to 1 and the others close to 0) indicates low uncertainty, while comparable probabilities for multiple classes suggest high uncertainty. Consequently, slices with lower uncertainty are assigned higher weights, and vice versa. For binary classification problems, the predicted probabilities for the two classes of the i -th slice of the j -th CT scan are denoted as $p_{i,j,1}$ and $p_{i,j,2}$. The weight for each slice is computed using (9):

$$w_{ij} = \max(p_{i,j,1}, p_{i,j,2}) - \min(p_{i,j,1}, p_{i,j,2}) \quad (9)$$

In this approach, the fuzzy integral operator assigns higher weights to slices that provide more confident information about the occurrence or absence of hemorrhage.

After determining the probability of each slice belonging to each class, referred to as the confidence vector, using a boosting neural network, and assigning a weight to each slice as the belief value, the slices of the CT scan images

TABLE III

PERFORMANCE METRICS OF DIFFERENT MODELS FOR SLICE-LEVEL ICH DETECTION ON THE TEST SET, INCLUDING GENERALIZED R-SQUARE, ENTROPY R-SQUARE, ROOT AVERAGE SQUARED ERROR (RASE), MEAN ABSOLUTE DEVIATION (MAD), AND LOG-LIKELIHOOD.

Model	Test Set				
	Generalized R-square	Entropy R-square	RASE	MAD	Log-Likelihood
VGG19	0.765	0.615	0.279	0.178	-2806
ResNet50	0.759	0.607	0.283	0.187	-2864
CCA	0.849	0.73	0.231	0.118	-1964
Pyramid ViT	0.754	0.602	0.287	0.18	-2905
DeiT	0.673	0.507	0.323	0.228	-3592
DenseNet	0.779	0.633	0.273	0.153	-2675
EfficientNetB6	0.652	0.484	0.334	0.241	-3761
Incep-ResNet	0.616	0.448	0.344	0.273	-4029
Xception	0.755	0.602	0.286	0.166	-2899
InceptionV3	0.767	0.618	0.278	0.169	-2784
MobileNetV2	0.704	0.541	0.312	0.21	-3345
Cross Attention	0.541	0.375	0.372	0.294	-4557
ResNet152	0.753	0.6	0.288	0.181	-2917
VGG16	0.819	0.687	0.251	0.138	-2278

are combined based on (8) to determine the final label of each scan. The proposed fuzzy integral operator, through the weighted aggregation of different CT image slices, improves hemorrhage detection accuracy while addressing the challenges associated with the standard version of the operator.

III. FINDINGS AND ANALYSIS

Since multiple CT scan images were typically recorded for each patient, to maximize the use of available scans and prevent data leakage, we included all scans from the same patient within the training data. The test data was designed to ensure subject independence. At the slice level, 80% of the data was designated for training, and 20% for testing. Considering that the training data included patients with multiple scans, this slice-level split corresponds to training the model on 50% of the patients and testing it on the remaining 50% at the patient level.

A. ICH Detection

The goal is to evaluate an intelligent model using CT scan images that can automatically detect the presence or absence of ICH. This is formulated as a binary classification problem, where the classes are defined as "Normal" and "ICH". Tables III and IV evaluate different models for slice-level ICH detection. Table III highlights regression metrics, where the CCA model achieved the best performance with the highest Generalized R-square (0.849) and lowest RASE (0.231) and MAD (0.118). In contrast, models like Cross Attention showed lower predictive capabilities.

Table IV focuses on classification metrics, with the CCA model again leading, achieving the highest Accuracy (0.911), Precision (0.943), and F1-score (0.93). VGG16 also performed well with an Accuracy of 0.896 and F1-score of 0.915. These results confirm the superior performance of the CCA model for ICH detection.

Fig. 7 illustrates the confusion matrix of the CCA model at the scan-level, where different slices were combined using the fuzzy integral operator based on uncertainty in the detection of ICH. With an accuracy of 98.4%, sensitivity of 98.4%, precision of 98%, specificity of 98.4%, and F1-score of 98.15%, the proposed approach demonstrates strong performance characteristics.

TABLE IV
EVALUATION METRICS OF DIFFERENT MODELS FOR SLICE-LEVEL ICH DETECTION, INCLUDING ACCURACY, PRECISION, SENSITIVITY, SPECIFICITY, AND F1-SCORE.

Model	Accuracy	Precision	Sensitivity	Specificity	F1-score
VGG19	0.878	0.911	0.883	0.893	0.897
ResNet50	0.874	0.912	0.872	0.895	0.891
CCA	0.911	0.943	0.917	0.925	0.93
Pyramid ViT	0.868	0.903	0.869	0.887	0.886
DeiT	0.84	0.874	0.84	0.859	0.857
DenseNet121	0.88	0.919	0.878	0.902	0.898
EfficientNetB6	0.824	0.859	0.823	0.845	0.841
Incep-ResNet	0.821	0.872	0.8	0.862	0.835
Xception	0.873	0.916	0.865	0.901	0.89
InceptionV3	0.879	0.912	0.882	0.895	0.897
MobileNetV2	0.846	0.882	0.846	0.866	0.864
Cross Attention	0.781	0.816	0.776	0.805	0.795
ResNet152	0.867	0.901	0.87	0.884	0.885
VGG16	0.896	0.924	0.907	0.905	0.915

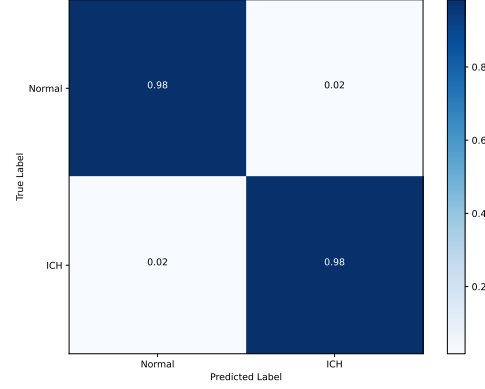


Fig. 7. Scan-level confusion matrix on test data for ICH detection.

B. SDH Detection

The aim here is to accurately identify the specific type of SDH. This binary classification includes "ASDH" and "CSDH" classes.

Table V focuses on regression-based metrics. The CCA model demonstrates the best performance with the highest Generalized R-square (0.85) and the lowest MAD (0.087). It significantly outperforms models like EfficientNetB6, which has the lowest Generalized R-square (0.629) and highest error metrics.

Table VI highlights classification metrics. The CCA model again leads with the highest Accuracy (0.913). The Incep-ResNet and Pyramid ViT models also perform well, while models like EfficientNetB6 and Xception show relatively lower performance.

In summary, the CCA model consistently achieves superior results across both regression and classification metrics, making it the most effective for slice-level ICH and SDH detection.

Fig. 8 depicts the confusion matrix of the CCA model at the scan-level, in which diverse slices are integrated using the proposed fuzzy integral operator to detect SDH. The accuracy of 98.8%, sensitivity of 98.7%, precision of 98.6%, specificity of 98.7%, and F1-score of 98.65% indicate that the classification model performs exceptionally well, with minimal misclassification, achieving near-perfect accuracy in both class predictions.

Table VII provides a comparison of this study with other research employing deep neural networks for ICH analysis.

TABLE V

PERFORMANCE METRICS OF DIFFERENT MODELS FOR SLICE-LEVEL SDH DETECTION ON THE TEST SET, INCLUDING GENERALIZED R-SQUARE, ENTROPY R-SQUARE, RASE, MAD, AND LOG-LIKELIHOOD.

Model	Test Set				
	Generalized R-square	Entropy R-square	RASE	MAD	Log-Likelihood
VGG19	0.778	0.634	0.276	0.156	-233
ResNet50	0.808	0.674	0.26	0.152	-207
CCA	0.85	0.734	0.722	0.087	-169
Pyramid ViT	0.813	0.691	0.245	0.119	-82
DeiT	0.765	0.627	0.272	0.163	-98
DenseNet121	0.807	0.672	0.257	0.156	-208
EfficientNetB6	0.629	0.462	0.34	0.235	-342
Incep-ResNet	0.841	0.72	0.233	0.126	-178
Xception	0.68	0.517	0.323	0.213	-184
InceptionV3	0.728	0.571	0.298	0.171	-273
MobileNetV2	0.74	0.585	0.295	0.164	-264
Cross Attention	0.683	0.53	0.303	0.197	-124
ResNet152	0.817	0.686	0.248	0.121	-199
VGG16	0.801	0.675	0.25	0.143	-86

TABLE VI

EVALUATION METRICS OF DIFFERENT MODELS FOR SLICE-LEVEL SDH DETECTION, INCLUDING ACCURACY, PRECISION, SENSITIVITY, SPECIFICITY, AND F1-SCORE.

Model	Accuracy	Precision	Sensitivity	Specificity	F1-score
VGG19	0.867	0.892	0.907	0.842	0.899
ResNet50	0.875	0.889	0.926	0.834	0.907
CCA	0.913	0.94	0.94	0.905	0.94
PVT	0.903	0.926	0.9	0.88	0.912
DeiT	0.879	0.893	0.878	0.921	0.885
DenseNet121	0.887	0.89	0.952	0.832	0.92
EfficientNetB6	0.815	0.845	0.863	0.781	0.854
Incep-ResNet	0.91	0.941	0.932	0.907	0.937
Xception	0.826	0.843	0.844	0.824	0.844
InceptionV3	0.861	0.882	0.907	0.827	0.894
MobileNetV2	0.855	0.878	0.901	0.822	0.889
Cross Attention	0.857	0.865	0.859	0.839	0.862
ResNet152	0.881	0.948	0.909	0.917	0.928
VGG16	0.898	0.911	0.905	0.885	0.908

Although prior studies have achieved commendable results, our approach demonstrates that integrating PCA and feature importance techniques not only reduces model complexity but also enhances accuracy. Notably, this also significantly improves the model's explainability.

IV. FUTURE RESEARCH DIRECTIONS

In the future, we aim to explore:

- An uncertainty-based fuzzy integral operator was utilized to fuse different slices of CT scan images at the decision level. Future studies can employ this operator at the data or feature level, allowing features extracted from various deep networks to be combined using this operator.
- Future research could investigate the optimal number of principle components, explore more sophisticated dimensionality reduction approaches, and optimize other hyperparameters.
- We excluded CT scan images that showed the occurrence of more than one type of hemorrhage. Future studies may define a new class for such cases.
- It is recommended to use clinical data such as blood pressure, age, and injury area to develop a rapid classification task aimed at identifying likely cases of hemorrhage.
- Future studies can focus on implementing the proposed system in a clinical setting to showcase its real-world potential and limitations.

V. CONCLUSION

ICH requires prompt and accurate diagnosis to ensure timely implementation of appropriate treatments. In this study, after feature extraction from CT scan images, the most informative

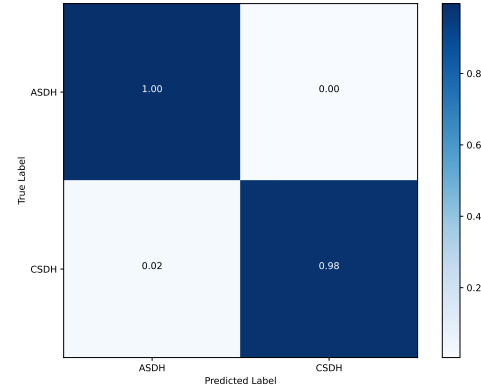


Fig. 8. Scan-level confusion matrix on test data for SDH detection.

TABLE VII
COMPARISON SUMMARY OF THE PROPOSED METHOD WITH EXISTING APPROACHES.

Work	Year	Dataset	Number of Samples	Objective	Deep Learning Model	Validation Strategy	Performance	
							AUC	F1-score
[35]	2022	Public	1469 scans	Normal/ICH	Pre-trained encoder-LSTM	Single-fold	AUC=0.988, F1-score = 0.933	
[36]	2022	Public	1540 scans	Normal/ICH	CNN with attention	Single-fold	AUC=0.988, F1-score = 0.957	
[9]	2023	Public	2501 slices	Normal/ICH	Weber Local Descriptor-Random Forest	Single-fold	Acc= 0.86, Sens= 0.87 Spec = 0.87	
[28]	2023	Public	18938 scans	Normal/ICH	EfficientNet's deep-learning technology	Single-fold	Acc= 0.94, Sens= 0.94 Spec = 0.94	AUC = 0.978
[4]	2023	Public	491 patients	Normal/ICH	Deep fuzzy Network	5-fold	Acc = 0.94, Pre = 0.938 Sens = 0.929, F1-score = 0.88	
[22]	2024	Public	1150 scans	Normal/ICH	An attention-based model with gaussian processes	Single-fold	Acc = 0.94, F1-score = 0.88, Prec = 0.82, AUC = 0.96	
[26]	2024	Public	457 scans	Normal/ICH	Patch FCN with dilated ResNet38	5-fold	AUC = 0.939	
[25]	2024	Private	642 patients	Normal/ICH	ML-powered Near-infrared spectroscopy based (mNIRS) system	Single-fold	Acc= 0.942, Sens = 0.948 Spec = 0.941	
[21]	2024	Public	70000 slices	Normal/ICH	Multiple instance learning with Gaussian Processes	Single-fold	Acc= 0.915, AUC = 0.94 F1-score = 0.902	
Our work	2024	Private	31596 slices (normal/ICH) 2785 slices (SDH types)	Normal/ICH ASDH/CSDH	Co-scale convolutional attention model with uncertainty-based fuzzy integral operator	Single-fold	Acc=0.984, Prec=0.98 Sens=0.984, Spec=0.984 F1-score = 0.981	
							Acc=0.988, Prec=0.98 Sens=0.987, Spec=0.987 F1-score = 0.986	

and most discriminative features were identified to feed into a hybrid neural network, enabling the classification of each slice into specific classes. Subsequently, we introduced a novel version of a fuzzy integral operator, enhanced with uncertainty-based weighting, to aggregate slices from CT scan images. The proposed approach, implemented on two separate datasets, demonstrated significant improvement in hemorrhage detection at the scan-level through the intelligent combination of multiple slices.

REFERENCES

- Y.-R. Chen, C.-C. Chen, C.-F. Kuo, and C.-H. Lin, "An efficient deep neural network for automatic classification of acute intracranial hemorrhages in brain ct scans," *Computers in Biology and Medicine*, vol. 176, p. 108587, 2024.
- A. Ferdi, S. Benierbah, A. Nakib, Y. Ferdi, and A. Taleb-Ahmed, "Quadratic convolution-based yolov8 (q-yolov8) for localization of intracranial hemorrhage from head ct images," *Biomedical Signal Processing and Control*, vol. 96, p. 106611, 2024.
- S. Nizarudeen and G. R. Shanmughavel, "Comparative analysis of resnet, resnet-se, and attention-based ranet for hemorrhage classification in ct images using deep learning," *Biomedical Signal Processing and Control*, vol. 88, p. 105672, 2024.
- P. Malik and A. Vidyarthi, "A computational deep fuzzy network-based neuroimaging analysis for brain hemorrhage classification," *IEEE Journal of Biomedical and Health Informatics*, 2023.
- S. Umapathy, M. Murugappan, D. Bharathi, and M. Thakur, "Automated computer-aided detection and classification of intracranial hemorrhage using ensemble deep learning techniques," *Diagnostics*, vol. 13, no. 18, p. 2987, 2023.

[6] S. Angkurawaranon, N. Sanorsieang, K. Unsrisong, P. Inkeaw, P. Sripan, P. Khumrin, C. Angkurawaranon, T. Vaniyapong, and I. Chitapanarux, "A comparison of performance between a deep learning model with residents for localization and classification of intracranial hemorrhage," *Scientific Reports*, vol. 13, no. 1, p. 9975, 2023.

[7] J. Lyu, Z. Xu, H. Sun, F. Zhai, and X. Qu, "Machine learning-based ct radiomics model to discriminate the primary and secondary intracranial hemorrhage," *Scientific Reports*, vol. 13, no. 1, p. 3709, 2023.

[8] F. Soheili, N. Delfan, N. Masoudifar, S. Ebrahimni, B. Moshiri, M. Glogauer, and E. Ghafar-Zadeh, "Toward digital periodontal health: Recent advances and future perspectives," *Bioengineering*, vol. 11, no. 9, p. 937, 2024.

[9] S. S. Gudadhe, A. D. Thakare, and D. Oliva, "Classification of intracranial hemorrhage ct images based on texture analysis using ensemble-based machine learning algorithms: A comparative study," *Biomedical Signal Processing and Control*, vol. 84, p. 104832, 2023.

[10] Y. S. Champawat, C. Prakash *et al.*, "Literature review for automatic detection and classification of intracranial brain hemorrhage using computed tomography scans," *Robotics, Control and Computer Vision*, pp. 39–65, 2023.

[11] M. Asif, M. A. Shah, H. A. Khattak, S. Mussadiq, E. Ahmed, E. A. Nasr, and H. T. Rauf, "Intracranial hemorrhage detection using parallel deep convolutional models and boosting mechanism," *Diagnostics*, vol. 13, no. 4, p. 652, 2023.

[12] M. Yeo, B. Tahayori, H. K. Kok, J. Maingard, N. Kutaiba, J. Russell, V. Thijss, A. Jhamb, R. V. Chandra, M. Brooks *et al.*, "Evaluation of techniques to improve a deep learning algorithm for the automatic detection of intracranial haemorrhage on ct head imaging," *European Radiology Experimental*, vol. 7, no. 1, p. 17, 2023.

[13] Y. Xiao, Y. Hou, Z. Wang, Y. Zhang, X. Li, K. Hu, and X. Gao, "Multi-scale perception and feature refinement network for multi-class segmentation of intracerebral hemorrhage in ct images," *Biomedical Signal Processing and Control*, vol. 88, p. 105614, 2024.

[14] N. M. Dashtaki, A. Mirahmadi, M. Fararouei, R. M. Dashtaki, M. Hoseini, and M. R. Nayeb, "The lag-effects of air pollutants and meteorological factors on covid-19 infection transmission and severity: Using machine learning techniques," *Journal of Research in Health Sciences*, vol. 24, no. 3, p. e00622, 2024.

[15] M. H. Chagahi, S. M. Dashtaki, B. Moshiri, and M. J. Piran, "Cardio-vascular disease detection using a novel stack-based ensemble classifier with aggregation layer, dowa operator, and feature transformation," *Computers in Biology and Medicine*, vol. 173, p. 108345, 2024.

[16] P. Hu, T. Yan, B. Xiao, H. Shu, Y. Sheng, Y. Wu, L. Shu, S. Lv, M. Ye, Y. Gong *et al.*, "Deep learning-assisted detection and segmentation of intracranial hemorrhage in noncontrast computed tomography scans of acute stroke patients: a systematic review and meta-analysis," *International Journal of Surgery*, vol. 110, no. 6, pp. 3839–3847, 2024.

[17] N. Delfan, P. K. Moghadam, M. Khoshnevisan, M. H. Chagahi, B. Hatami, M. Asgharzadeh, M. Zali, B. Moshiri, A. M. Moghaddam, M. A. Khalafi *et al.*, "Ai-driven non-invasive detection and staging of steatosis in fatty liver disease using a novel cascade model and information fusion techniques," *arXiv preprint arXiv:2412.04884*, 2024.

[18] N. Delfan, M. Shahsavari, S. Hussain, R. Damaševičius, and U. R. Acharya, "A hybrid deep spatiotemporal attention-based model for parkinson's disease diagnosis using resting state eeg signals," *International Journal of Imaging Systems and Technology*, vol. 34, no. 4, p. e23120, 2024.

[19] H. Lee, S. Yune, M. Mansouri, M. Kim, S. H. Tajmir, C. E. Guerrier, S. A. Ebert, S. R. Pomerantz, J. M. Romero, S. Kamalian *et al.*, "An explainable deep-learning algorithm for the detection of acute intracranial haemorrhage from small datasets," *Nature biomedical engineering*, vol. 3, no. 3, pp. 173–182, 2019.

[20] M. H. Chagahi, S. M. Dashtaki, N. Delfan, N. Mohammadi, A. Samari, B. Moshiri, M. J. Piran, U. R. Acharya, and O. Faust, "Enhancing osteoporosis detection: An explainable multi-modal learning framework with feature fusion and variable clustering," *arXiv preprint arXiv:2411.00916*, 2024.

[21] F. M. Castro-Macías, P. Morales-Álvarez, Y. Wu, R. Molina, and A. K. Katsaggelos, "Hyperbolic secant representation of the logistic function: Application to probabilistic multiple instance learning for ct intracranial hemorrhage detection," *Artificial Intelligence*, vol. 331, p. 104115, 2024.

[22] J. Pérez-Cano, Y. Wu, A. Schmidt, M. López-Pérez, P. Morales-Álvarez, R. Molina, and A. K. Katsaggelos, "An end-to-end approach to combine attention feature extraction and gaussian process models for deep multiple instance learning in ct hemorrhage detection," *Expert Systems with Applications*, vol. 240, p. 122296, 2024.

[23] T. D'Angelo, G. M. Bucolo, T. Kamareddine, I. Yel, V. Koch, L. D. Gruenewald, S. Martin, L. S. Alizadeh, S. Mazzotti, A. Blandino *et al.*, "Accuracy and time efficiency of a novel deep learning algorithm for intracranial hemorrhage detection in ct scans," *La radiologia medica*, pp. 1–8, 2024.

[24] C. Sindhura, M. Al Fahim, P. K. Yalavarthy, and S. Gorthi, "Fully automated sinogram-based deep learning model for detection and classification of intracranial hemorrhage," *Medical Physics*, vol. 51, no. 3, pp. 1944–1956, 2024.

[25] J. Shah, K. Vithalapara, S. Malik, A. Lavania, S. Solanki, and N. S. Adhvaryu, "Human factor engineering of point-of-care near infrared spectroscopy device for intracranial hemorrhage detection in traumatic brain injury: A multi-center comparative study using a hybrid methodology," *International Journal of Medical Informatics*, vol. 184, p. 105367, 2024.

[26] E. Lin and E. L. Yuh, "Semi-supervised learning for generalizable intracranial hemorrhage detection and segmentation," *Radiology: Artificial Intelligence*, vol. 6, no. 3, p. e230077, 2024.

[27] M. Ragab, R. Salama, F. S. Alotaibi, H. A. Abdushkour, and I. R. Alzahrani, "Political optimizer with deep learning based diagnosis for intracranial hemorrhage detection," *IEEE Access*, 2023.

[28] L. Cortés-Ferre, M. A. Gutiérrez-Naranjo, J. J. Egea-Guerrero, S. Pérez-Sánchez, and M. Balcerzyk, "Deep learning applied to intracranial hemorrhage detection," *Journal of Imaging*, vol. 9, no. 2, p. 37, 2023.

[29] C. Li, Z. Xi, G. Jin, W. Jiang, B. Wang, X. Cai, and X. Wang, "Deep-learning-enabled microwave-induced thermoacoustic tomography based on resattu-net for transcranial brain hemorrhage detection," *IEEE Transactions on Biomedical Engineering*, vol. 70, no. 8, pp. 2350–2361, 2023.

[30] E. P. Klement, R. Mesiar, and E. Pap, "A universal integral as common frame for choquet and sugeno integral," *IEEE transactions on fuzzy systems*, vol. 18, no. 1, pp. 178–187, 2009.

[31] H. Tahani and J. M. Keller, "Information fusion in computer vision using the fuzzy integral," *IEEE Transactions on systems, Man, and Cybernetics*, vol. 20, no. 3, pp. 733–741, 1990.

[32] L. Horanská and A. Šipošová, "A generalization of the discrete choquet and sugeno integrals based on a fusion function," *Information Sciences*, vol. 451, pp. 83–99, 2018.

[33] M. Ayub, "Choquet and sugeno integrals," 2009.

[34] M. Sugeno, "A way to choquet calculus," *IEEE Transactions on Fuzzy Systems*, vol. 23, no. 5, pp. 1439–1457, 2014.

[35] S. Kyung, K. Shin, H. Jeong, K. D. Kim, J. Park, K. Cho, J. H. Lee, G. Hong, and N. Kim, "Improved performance and robustness of multi-task representation learning with consistency loss between pretexts for intracranial hemorrhage identification in head ct," *Medical Image Analysis*, vol. 81, p. 102489, 2022.

[36] M. López-Pérez, A. Schmidt, Y. Wu, R. Molina, and A. K. Katsaggelos, "Deep gaussian processes for multiple instance learning: Application to ct intracranial hemorrhage detection," *Computer Methods And Programs In Biomedicine*, vol. 219, p. 106783, 2022.